# In-situ XRD study of a Chromium doped LiNi0.5Mn1.5O4 cathode for Li-ion battery

CHLADIL, L.; KUNICKÝ, D.; KAZDA, T.; VANÝSEK, P.; ČECH, O.; BAČA, P.

Journal of Energy Storage
Volume 41, September 2021, 102907, Pages 1-15

ISSN: 2352-152X

DOI: https://doi.org/10.1016/j.est.2021.102907

Accepted manuscript

# In-situ XRD Study of a Cr Doped $LiNi_{0.5}Mn_{1.5}O_4$ Cathode for Li-ion Battery

L. Chladil[a,b], D. Kunický[a], T. Kazda[a,b], P. Vanýsek[a,b], O. Čech[a,b] and P. Bača [a,b]

[a] Department of Electrical and Electronic Technology, Brno University of Technology, Technicka 10, 616 00 Brno, Czech Republic

[b] Centre for Research and Utilization of Renewable Energy, Faculty of Electrical Engineering and Communication, BUT, Technicka 10, 616 00 Brno, Czech Republic

## Abstract

This paper deals with structural (*in-situ* XRD) and electrochemical characterization of high-voltage lithium-ion cathode materials $LiMn_2O_4$ (LMO), $LiNi_{0.5}Mn_{1.5}O_4$ (LNMO), and $LiCr_{0.1}Ni_{0.4}Mn_{1.5}O_4$ (LCNMO) prepared by solid-state synthesis. Structural *in-situ* X-ray diffraction spectra were measured by an affordable Rigaku diffractometer. Our synthesis route produced the samples with similar morphologies where the average particle sizes were 1.11 μm and 1.46 μm for LNMO and LCNMO respectively. Results of the Rietveld analysis brought detailed insight into two-phase structure transitions for LMO and three-phase transitions for LNMO and LCNMO. XRD study revealed differences in the structural behavior of LMO and LNMO prepared by solid-state synthesis compared to the results of other authors using the sol-gel synthesis route. In the case of chromium-doped LNMO, our results indicate ability of the chromium metal to effectively reduce $Mn^{3+}$ content while the ordering of the structure increases. Chromium doping also promotes a larger lattice parameter in a fully delithiated state than in the case of undoped LNMO. Therefore, lowering of the volume changes was observed and faster phase II/III transition taking place, when $Ni^{3+}/Ni^{4+}$ redox pair was oxidized, was also identified. Cr doping of LNMO also promotes the reaching the lattice parameters of phases in both phase transitions and thus could reduce the internal stress of active material under high C-rate cycling. Results thus suggested that chromium doping can improve the stability of the inner structure and performance at higher charging C-rates even though the structure goes through a three-phase region during charging as undoped LNMO. The evaluation of diffusion coefficients of Cr-doped LNMO revealed increased diffusivity in a full discharge state and as the cathode underwent the cycling the differences in diffusivity seemed to be more pronounced.

## Introduction

Lithium-ion batteries are progressively being deployed in electric vehicles (EVs) and in a grid energy storage where a long lifetime is a significant requirement. Majority of car drivers travel daily only between 0-80 km while the range of the EVs is about 400 km. This would seem already sufficient range. However, there is an increased application of autonomous vehicles and electric-powered trucks where the 400 km range might be close to the daily demand of 100 % DoD [1]. From a long-term stability point of view, deep cycling significantly accelerates irreversible electrode changes especially in high-voltage Li-ion systems, and thus promotes fast capacity decay. Many researchers are therefore targeting ways to stabilize the structures by doping by various elements to increase the battery life-span while utilizing fully its capacity.

Very well-known electrode material $LiFePO_4$ was widely used in EVs, hybrid EVs, etc. This phospho-olivine material has been first introduced by Padhi et al. in 1997 [2]. It is considered to be better than $LiCoO_2$ in some aspects such as safety at high temperatures, overcharges, and in its non-toxicity [3].

Other materials that are promising better performance are high voltage materials based on $LiMn_2O_4$, mainly doped with 0.5 mole percent of nickel – $LiNi_{0.5}Mn_{1.5}O_4$ (LNMO) [4] [5] [6]. This material has higher redox potential (around 4.7 V) because of the transition of $Ni^{2+}$ to $Ni^{4+}$ [6] and higher gravimetric energy density (around 700 Wh/kg). It is also more environmentally friendly than $LiCoO_2$ as it does not contain potentially toxic and rare cobalt. LNMO generally could be synthesized as an ordered structure and a disordered one which exhibit $P4_332$ space group and Fd-3m respectively. In the first case, Ni atoms occupy 4a and 12d sites, whereas in the case of Fd-3m nickel is randomly distributed in the octahedral 16d sites [7]. Each phase exhibits different parameters such as conductivity, $Li^+$ diffusivity, capacity retention at high C-rate and also different long-term performance [8] [7]. Effect of different Ni content in $LiNi_xMn_{2-x}O_4$ was published in a complex study developed by Duncan et al. [9]. They found that the transition between the ordered and disordered structure proceeds in a narrow $Mn^{3+}$ content window that was almost linearly dependent on the amount of Ni substitution for Mn. Because the presence of $Mn^{3+}$ is associated with dissolution of active mass and therefore with a gradual fade of the electrode capacity [8], therefore there are general attempts to reduce the amount of $Mn^{3+}$. However, its presence is also accompanied by beneficial oxygen deficiency in the structure that improves the electronic conductivity in the bulk. The other important aspect of high-voltage LNMO spinels is so-called disordering which is generated by randomized occupancy of nickel on the manganese 16d site positions. The main increase in disordering was found for $0.35>x>0.4$ in $LiNi_xMn_{2-x}O_4$ and typically developed $LiNi_{0.5}Mn_{1.5}O_4$ with synthesis temperature around 700 °C and slow cooling exhibited ordered structure with a low amount of $Mn^{3+}$ [9]. Such ordered structure shows good cyclability but worse capacity retention in comparison to disordered one prepared by fast cooling in the final stage of synthesis. Disordering of the structure by post-synthesis temperature treatment is one way how to influence the disordering without significant increase of $Mn^{3+}$ which brings the long-term material instabilites.

LNMO generally suffers from the dissolution of manganese into the electrolyte during cycling at higher temperatures. This leads to a capacity decrease and worse structural stability [10]. This could be caused by the Jahn-Teller distortion which occurs in octahedral and tetrahedral compounds. The observation was published in 1937 by H. A. Jahn and E. Teller [11] and states that in an electronically degenerate state, a nonlinear molecule undergoes distortion to remove the degeneracy by lowering the symmetry and thus by lowering the energy. Although known for eight decades, the details of the Jahn-Teller distortion remained elusive. Another problem of Mn-based oxides is the oxygen release during higher temperatures. This phenomenon can be expressed for example as $LiMn_2O_4 \rightarrow LiMnO_2 + 1/3\ Mn_3O_4 + 1/3\ O_2$. There is a phase transition during charging and discharging which leads to significant structural changes, thus leading to worse structural stability during cycling [12].

There were used many different doping elements to try to improve LMO or LNMO performance. LMOs doping by phosphorus drastically improved cyclability and rate capability even at elevated temperatures [13], doping by zinc [14] also improved cyclability, and the increasing concentration of zinc provided long-term cycle stability and superior reproducibility. Materials moderately doped by molybdenum [10] had increased structural stability even at higher temperatures. The double doping by indium and sulfur [15] optimized the cycle stability, discharge capacity, and high rate discharge ability. Cycling performance and specific capacity improvement were done by doping with chromium [16]. Promising doping materials are from the lanthanides series. For example, gadolinium [17] has significantly improved structural stability, stability at high discharge

rates, and reversible capacities, which was attributed to suppression of the Jahn-Teller distortion. Exceptional structural stabilization was achieved by scandium doping [18]. There are also studies of new materials ranging from vanadium oxides [19] [20] to organic compounds [21] [22].

As charging and discharging continue in lithium-ion batteries, the crystallographic structure of the electrodes is changing. This has a significant effect on the overall performance of the batteries. The charging of cathodes is tied to the decrease of lithium ions as the lithium ions leave the structure. From a structural viewpoint, a small decrease of lithium concentration leads to a decrease of ion occupancy that could change the lattice constant only by a small amount. A gradual loss of lithium planes during delithiation leads to a complete transformation of the cathode materials structure [8] [9] [23]. Phase transition is different for ordered and disordered LNMO and also varies with different $Mn^{3+}$ content. Whereas the well-ordered structure exhibits three-phase transition during lithiation/delithiation [9], disordered structure with a high amount of $Mn^{3+}$ is manifested by one two-phase transition. Our analysis of available literature shows that two-phase transition was generally measured especially for structures with $Mn^{3+}$ content around 20 % or more [23] [24].

Delithiation is in any case accompanied by significant changes in the lattice dimensions regardless of the presence of the transitional phase and this results in volume changes of materials during charging and discharging. These changes can be seen from X-ray diffractograms and can be calculated by the Rietveld analysis. It is also known that volume changes directly influence the long-term stability of the materials, and therefore a precise measurement of these structural parameters in a different state of charge (SoC) is essential for assessing the expectations for long-term usability [25].

Yoon et al. found out that the structural stability of the cathode material is affected by the post-calcination cooling rate [26]. Gao et al. improved stability by annealing the base material, prepared by the solid-state method, for two hours after fine grinding [24]. Also, the structure itself on a micro-scale affects stability [27] [28].

A recent study by Kondracki et al. [23] used copper to verify the stabilization of the structure. This was successfully verified as the volume changes during charging were only 3.3 %. It is attributed to the reduction of the free volume within the unit cell and improved kinetics of lithium diffusion.

Our structural and electrochemical study is focused on the usage of chromium in $LiNi_{0.5}Mn_{1.5}O_4$ and how it can help stabilize the structural properties and how it could influence the diffusion properties of the cathode. The main benefit of this work lies mainly in the comparison of pure LNMO and Cr-doped LNMO prepared by the same synthesis route which allows clear identification of the effect of chromium on all properties of LNMO masses such as $Mn^{3+}$, the structure arrangement, the position of phase transitions and transition speed, diffusivity of $Li^+$, etc.

The results in this paper were obtained using the basic diffractometer Rigaku Miniflex 600HR, which is widely used in industrial quality inspection, equipped with an *in-situ* electrochemical cell attached to the diffractometer positioning system. Using X-ray diffractometry in connection with electrochemical impedance spectroscopy (EIS) can bring deeper insight into the electrochemical processes and structural changes taking place inside the materials and thus can provide accurate feedback on new ways of material optimization.

## Experimental

$LiMn_2O_4$ (LMO), $LiNi_{0.5}Mn_{1.5}O_4$ (LNMO), and $LiCr_{0.1}Ni_{0.4}Mn_{1.5}O_4$ (LCNMO) were prepared by a solid-state synthesis. LMO was produced by NEI Corporation

distributed by Sigma-Aldrich and LNMO and LCNMO were prepared by own solid-state synthesis from carbonates ($Li_2CO_3$ and $MnCO_3$) and oxides (NiO and $Cr_2O_3$) precursors obtained also from Sigma-Aldrich. Preparation is described in detail in [29] and [30]. Materials were prepared by a two-step solid-state synthesis process contain annealing at 600 °C for 10 hours and annealing at 900 °C for 15 hours. Cooling was realized by opening the furnace and therefore the cooling had a higher speed in the first phases of cooling and within 1.5 hours the samples reached approx. 350 °C.

Electrodes were prepared from the slurry containing active material which was mixed in the mass ratio 80:10:10 with polyvinylidene difluoride (PVDF) binder and Super-P carbon. N-methyl-2-pyrrolidone (NMP) has been added to create a dense pasty mass.

Electrodes for galvanostatic and EIS testing were prepared from electrode slurry by doctor-blade casting on aluminum foil. Then the electrodes were dried and pressed by the pressure of 31.4 $kN/cm^2$. A disc electrode with a diameter of 18 mm (2.54 $cm^2$) was cut out of the coated aluminum foil and investigated in El-Cell© ECC-Std electrochemical test cell. The cell assembly was carried out in an M-Braun argon-filled glove box. Metallic lithium was used as the counter electrode and a 1.5 $mol \cdot dm^{-3}$ $LiPF_6$ EC:DMC 1:2 w/w electrolyte was soaked in a glass fiber separator. Galvanostatic charge and discharge cycling were utilized as a method for the investigation of capacity retention with the potential window from 3.0 V to 5.1 V versus $Li/Li^+$. Polarization and impedance studies were performed on Biologic VSP potentiostat.

For the in-situ XRD study, the slurry was stirred with a magnetic stirrer for 24 hours and then coated onto an expanded thin metal aluminum foil stamped in the shape of a coin and dried at 50 °C for 1 hour. After drying the second layer of the active substance was applied, it was followed by drying at 50 °C for 1 hour and then followed by drying at 105 °C for at least 24 hours. After thorough drying, the sample was pressed by pressure 24.5 $kN/cm^2$. The assembly of the cell was done in an argon-filled glove box Jacomex. The electrode was then put into an ECC-Opto-Std cell by El-Cell® that has been adapted for direct insertion into the chamber of the powder diffractometer Rigaku Miniflex 600 HR. A separator made from glass fibers was used and the cell was filled by electrolyte EC:DMC (1:1) with 1 $mol \cdot dm^{-3}$ $LiPF_6$. A higher EC:DMC ratio was preferred for short-term in-situ measurement due to the better conductivity of the mixture [31]. Metal lithium was used as both the reference and counter electrodes (0.75 mm thick foil).

Charging proceeds inside of the diffractometer chamber, as shown in Figure 1, in the range of 10-110 degrees. As an X-ray transparent window was used a Kapton foil. The charging rate was set to be 0.05 C with the overall duration around 20 hours. X-ray diffractograms were obtained *operando*.

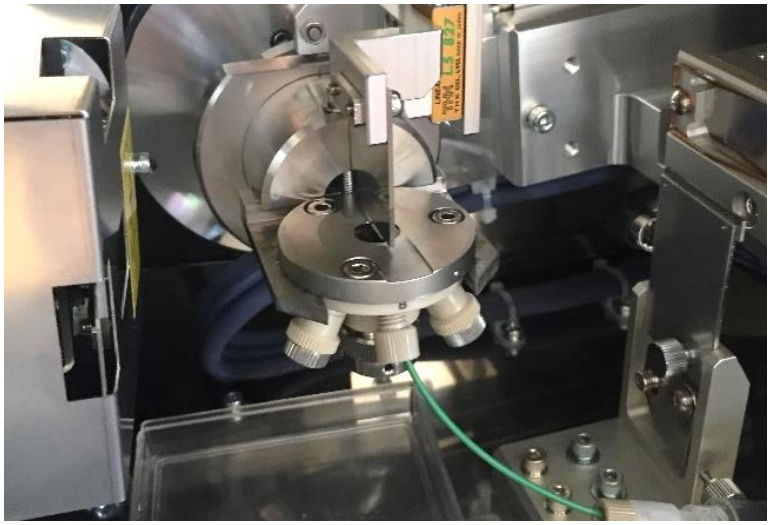

*Figure 1 Modified Opto-Std cell by El-Cell mounted in the chamber of the powder diffractometer*

## Structure and morphology of LNMO and LCNMO

Figure 2 shows the SEM images of LNMO and LCNMO particles. Both powders contain clusters of octahedral particles whose diameters vary approximately from 0.5 µm to 3 µm. For a better characterization of the powders, SEM images using the ImageJ (National Institutes of Health) program were analyzed and diameters of the selected group of particles were measured for both samples. Measured particle sizes were divided into bins and particle profile distribution in Figure 3 was compiled.

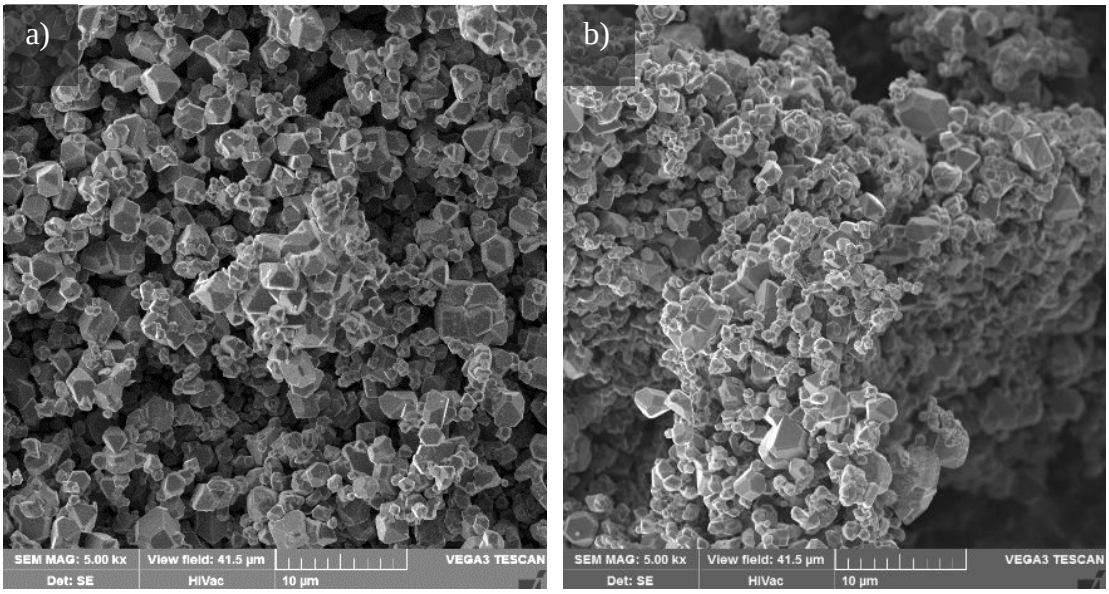


*Figure 2: SEM image of a) $LiNi_{0.5}Mn_{1.5}O_4$ particles and b) $LiCr_{0.1}Ni_{0.4}Mn_{1.5}O_4$ particles.*

The particle size profile revealed that LNMO has basically smaller particles than the Cr doped one and most of the particles are in the range from 0.7 µm to 1.1 µm, and 1.1 µm to 1.7 µm respectively. The average particle diameter is 1.11 µm for LNMO and 1.46 µm for LCNMO. The surface area of the powders can be calculated using Eq. 1:

$$A = \frac{\sum S_p}{\sum m_p} \qquad (1)$$

where $A$ is the surface of the powder, $S_p$ is the surface of each measured particle selected for particle profile analysis which is calculated from their diameters (assuming a spherical particle shape) and $m_p$ is the mass of each analyzed particle. Calculated values of powder surface and parameters of the electrode for EIS investigation (weight of active material $m_{el}$ and calculated area of active material/electrolyte interface $A_{el}$ for each electrode) are summarized in Table 1. Although the surface area was not determined by the much more precise BET technique, our calculated values are in good agreement with the BET surface parameter of samples of other authors [32] who synthesized the powders with similar particle diameter and published the BET surfaces slightly above 1.0 $m^2g^{-1}$.

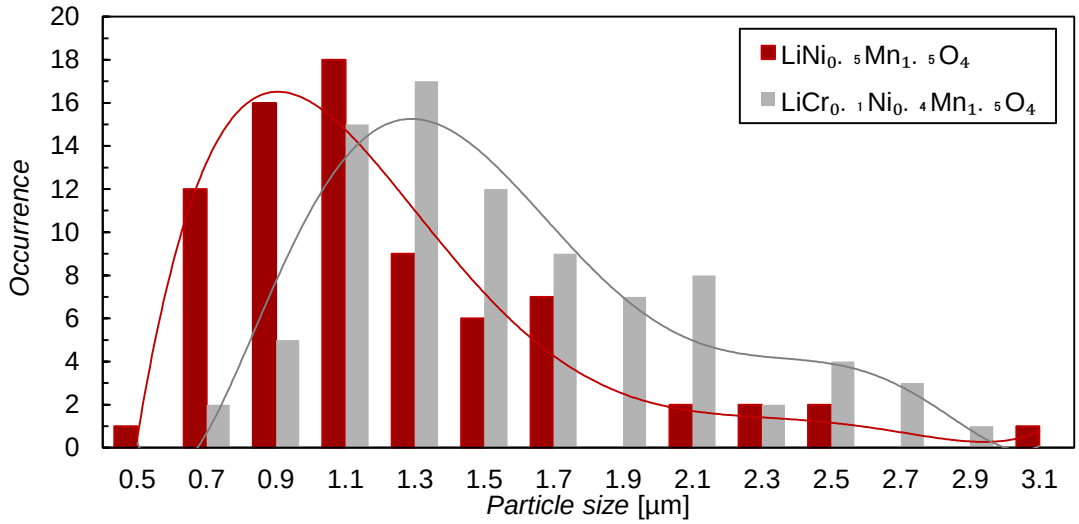


*Figure 3 Distribution of particle sizes of $LiNi_{0.5}Mn_{1.5}O_4$ (LNMO) and $LiCr_{0.1}Ni_{0.4}Mn_{1.5}O_4$ (LCNMO)*

*Table 1 Calculated parameters of LNMO and LCNMO powders*

| Material | $d_{avg}$ [µm] | $A$ [$m^2g^{-1}$] | $m_{el}$ [g] | $A_{el}$ [$cm^2$] |
|---|---|---|---|---|
| **LNMO** | 1.11 | 0.865 | $4.61 \cdot 10^{-3}$ | 39.9 |
| **LCNMO** | 1.46 | 0.765 | $5.76 \cdot 10^{-3}$ | 44.1 |

## Crystallographic study

The structural characterization was done first on pristine materials. All samples LMO, LNMO, and LCNMO indicated a symmetric Fd-3m space group which is, unlike primitive cubic structure ($P4_332$), typical for the synthesis where the temperature exceeds 700 °C. The results of the lattice cell parameter $a$ and the lattice volumes from the initial Rietveld analysis for each analyzed structure are shown in Table 2 and the values agree with literature [23] [33]. It can be seen that addition of chromium ions does not change the structure parameters significantly. According to [34] chromium doping of LMO leads to a gradual reduction of lattice parameter $a$ as the concentration of chromium increases because of the replacement of the larger $Mn^{3+}$ by smaller $Cr^{3+}$ ions. This resulted in a 0.38 % change of the lattice constant when the $Cr^{3+}$ replaced 25 % of $Mn^{3+}$ positions. When we replace the same amount of $Mn^{3+}$ ions with $Ni^{3+}$, the lattice parameter is reduced by 0.61 %. Replacement of $Ni^{3+}$ by $Cr^{3+}$ at a higher level could lead to an increase of the parameters $a$ to some extent. In this state, the part of larger $Ni^{3+}$ ions are replaced by smaller $Cr^{3+}$ but without noticeable changes in the lattice constant which in turn could lead to better permeability for $Li^+$ ion during lithiation/delithiation.

XRD patterns of pristine materials are shown in Figure 4. There were detected $Mn_2O_3$ impurities in the LMO pattern. No impurities were detected in other patterns. It can

be seen that all patterns display diffraction peaks with their attributed lines at 18° (111), 36° (311), 38° (222), 44° (400), 48° (331), and 64° (440). The intensity ratios of (311) and (400) peaks vary from sample to sample which indicates the different occupancy of cations between tetrahedral and octahedral 16d sites of the spinel structure. The ratio is lower for $LiCr_{0.1}Ni_{0.4}Mn_{1.5}O_4$ indicating that the chromium ions occupy mainly the octahedral positions. This is consistent with the study [35] and the same tendency of occupation was reported also in the case of Cu-doping of LNMO [23]. Other authors [33] assume that in fact, two atoms of $Cr^{3+}$ replace a pair $Ni^{2+}$ + $Mn^{4+}$ and thus help to maintain the $Mn^{4+}$ oxidation state unchanged which in turn leads to a longer life-span of the structure. Moreover, the substitution of Cr can gain the structure disorder in such a way, that $Ni^{2+}$ and $Mn^{4+}$ are ordered on octahedral sites at a shorter range only [36] and this is expected to increase the diffusion properties of the bulk.

*Table 2. Structural characterization of pristine materials LMO, LNMO, and LCNMO.*

| **Material** | **Space group** | **Lattice constant [Å]** | **Lattice volume [Å$^3$]** |
|---|---|---|---|
| $LiMn_2O_4$ | Fd-3m | a= 8.212 | 557.03 |
| $LiNi_{0.5}Mn_{1.5}O_4$ | Fd-3m | a= 8.171 | 545.73 |
| $LiCr_{0.1}Ni_{0.4}Mn_{1.5}O_4$ | Fd-3m | a= 8.169 | 545.79 |

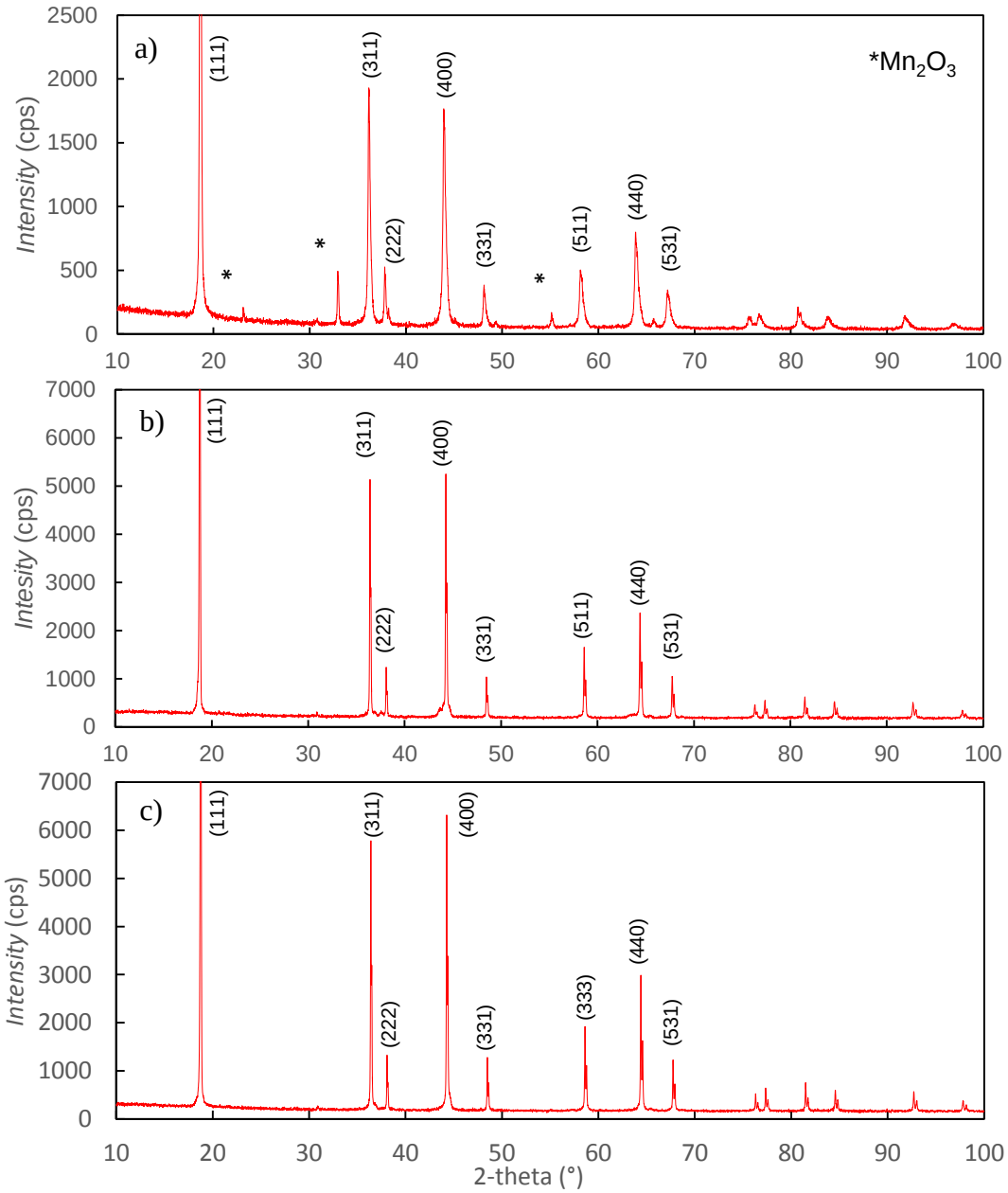


*Figure 4 XRD pattern of pristine a) LMO with marked $Mn_2O_3$ impurity phase b) LNMO and c) Cr-doped LNMO (LCNMO)*

Figure 5, Figure 7, and Figure 10 display the part of the XRD patterns for LMO, LNMO, and LCNMO, where the changes in structure can be easily read. Measured diffraction spectra were analyzed by the Rietveld refinement and the results of the lattice constant in dependence on the state of lithiation $x_{Li}$ are shown in Figure 6, **Error! Reference source not found.**, and Figure 12 for each analyzed sample. The summary of the lattice parameters in lithiated (0 % SoC) and delithiated (100 % SoC) states for all measured materials is shown in Table 3. At the start of the measurement, the cathode materials are from the synthesis fully lithiated and thus the bottom lines in Figure 5 represent the state, where $x_{Li}$ = 1. At the fully charged state – top line – the lattice parameters reach a value $a$ = 8.05 Å which can be attributed, according to [37], to a 10 % of residual lithium concentration. Therefore, we marked this state as $x_{Li}$ = 0.1 at 100 % SoC of the electrode. Because each material was charged a slightly different length of time, the number of XRD scans was also different and varied from 20 scans for LMO to 22 scans for LNMO. Therefore, between

each scan of spectra, the $x_{Li}$ value decreases about 0.045 for LMO, about 0.039 for LNMO, and about 0.041 for Cr-doped LNMO. A fully delithiated state was determined by a noticeable increase in the charging voltage in the final stages where there are no longer any changes in the measured spectra. The marked aluminum peak is from an expanded metal current collector and besides it indicates that the information about cathode structure is obtained from the entire thickness of the electrode layer. The aluminum peak has a stable position which excluded any position changes of the electrode during XRD measurement.

The presented X-ray spectra in Figure 5 and Figure 6 for LMO correspond to the experiments of other authors [23] who reported the two-phase transition region. Diffraction patterns of the measured LMO material show the stable one-phase $Li_xMn_2O_4$ structure during charging until $x_{Li}$=0.495 (55 % SoC) where the presence of the two-phase region appears (highlighted with red lines). The movement of the peaks (311) and (222) to the right side indicates the diminishing lattice parameters. Until 55 % SoC, only the reduction of the Li-rich phase has taken place. Following the rise of SOC leads to a gradual appearance of the new $MnO_2$ phase representing a fully charged state and when the electrode reaches 85 % SoC $x_{Li}$=0.765, the Li-rich phase fully disappeared and the cathode was transformed again to a single-phase region where only λ-$MnO_2$ was present. Our results fully correspond to LMO prepared by the sol-gel synthesis route [23]. The two-phase region thus exists roughly between $0.5 < x_{Li} < 0.23$ for LMO.

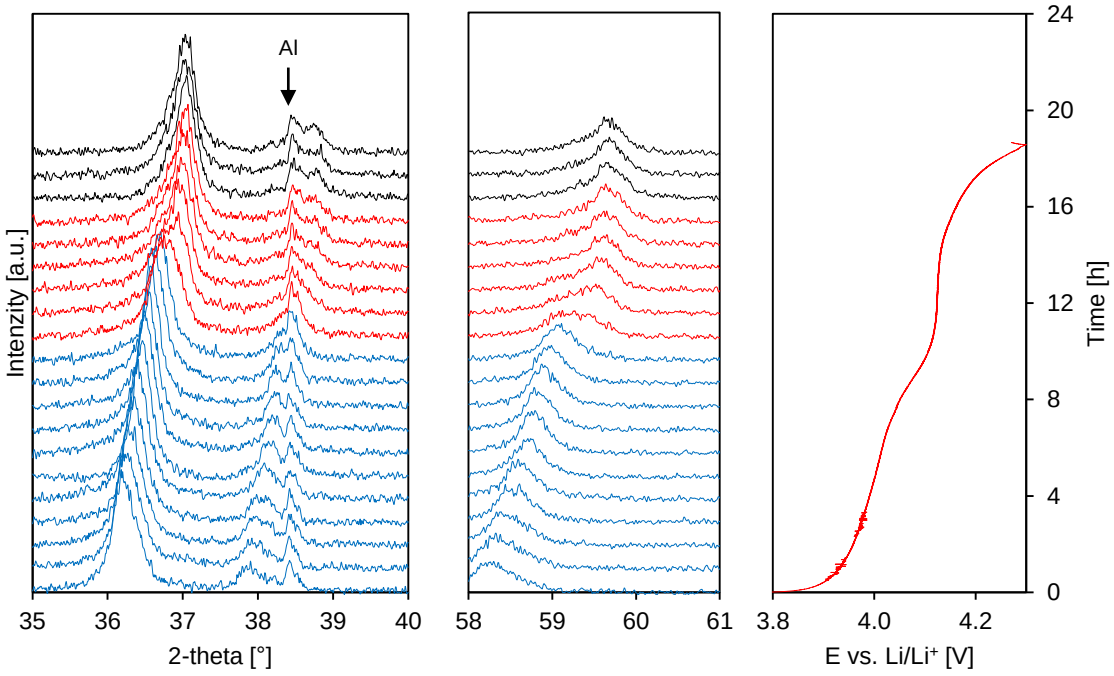


*Figure 5 XRD patterns (left) of LMO obtained during delithiation process and corresponding voltage plateau (right) measured at C/20 load. Blue and black lines correspond to the occurrence of single-phase regions when only the charged and discharged phases were detected; red one indicates the presence of both phases simultaneously.*

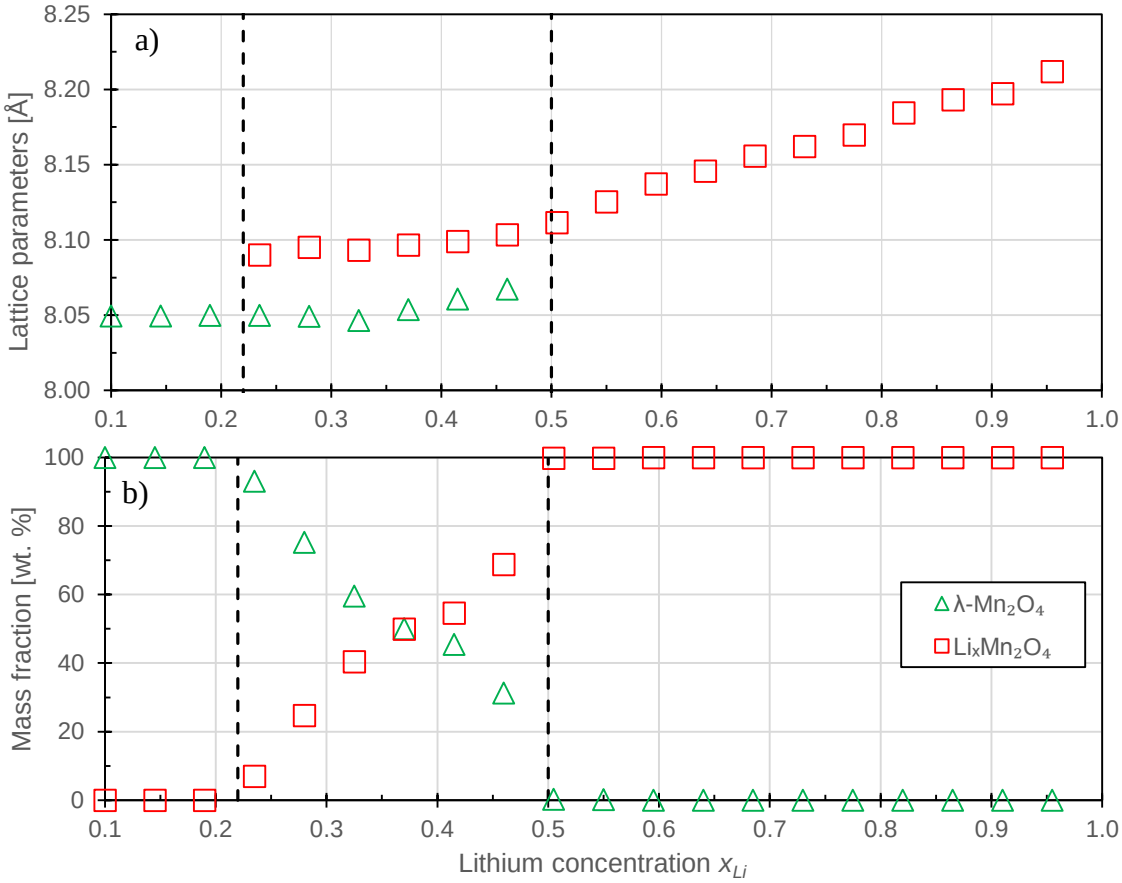


*Figure 6 Results from the Rietveld analysis of XRD spectra for LMO for a different state of lithiation $x_{Li}$: a) Lattice parameter changes of $Li_xMn_2O_4$ corresponding to discharged state and λ-$Mn_2O_4$ for charged state b) Content ratio changes of the identified phases.*

**Structure ordering and $Mn^{3+}$ content of LNMO and Cr-doped LMNO**

LNMO structure ordering is closely linked to $Mn^{3+}$ occurrence and the potential difference between $Ni^{2+}/Ni^{3+}$ and $Ni^{3+}/Ni^{4+}$ redox couples. Therefore, estimation of $Mn^{3+}$ and the effect of Cr doping on potential separation of nickel redox couple have to be evaluated and discussed at first. The Amount of $Mn^{3+}$ could be generally estimated from the area of cyclic voltammetry peak around 4.1 V and in our case also from galvanostatic curves (Figure 7 and Figure 10) can be derived from the capacity of the initial galvanostatic plateau of delithiation – i.e. capacity from start delithiation to reaching 4.4 V. Calculation suggests that our disordered LNMO contains approx. 14.4% $Mn^{3+}$ in the case of LNMO and 9.1 % $Mn^{3+}$ in the case of Cr doped LNMO. It implied that in our study 20 % replacement of nickel by chromium reduced the $Mn^{3+}$ by almost 37 % in the same solid-state synthesis route.

Analysis of galvanostatic potential plateau for different nickel redox couples revealed that the pure LNMO exhibits 58 mV separation while Cr-doped LNMO exhibits 66 mV. Both materials, therefore, can be considered as disordered ones and chromium addition tends to increase the structure disorder and thus influence the diffusivity in a beneficial way. The real effect of chromium on diffusion properties will be the subject of the second part of this study dedicated to the lithium diffusivity measurement using the electrochemical impedance spectroscopy investigation technique.

**Structural changes of LNMO**

*Operando* X-ray spectra of LNMO shown in Figure 7 and Figure 8 exhibits different behavior than LMO. At the first glance, the diffraction peak around 37 ° also

points to a two-phase transition that could correspond to findings of authors [23] [24], but in a detailed analysis of the spectra changes in range 58° - 61° (2-theta) corresponding to Bragg reflection from (511) plane, we can identify the three-phase transition. The gradual transition of structure using three phases was reported by [36] [38] [9] and [8]. Three-phase transition is typical for well-ordered LNMO with a low-amount of $Mn^{3+}$ (typically $LiNi_xMn_{2-x}O_4$, where x varies from 0.4 to 0.5, synthesized under 700 °C) or for partially disordered structure prepared by post-synthesis annealing of the well-ordered sample at 720 °C [9]. All three phases exhibit cubic Fd-3m symmetry. Phase I in a fully lithiated state corresponds to $LiNi_{0.5}Mn_{1.5}O_4$, phase II can be attributed to partially delithiated $Li_{0.5}Ni_{0.5}Mn_{1.5}O_4$ and Phase III is fully charged $Ni_{0.5}Mn_{1.5}O_4$. For Rietveld refinement analysis we adjusted the occupancy of Li to 0.5 for phase II in comparison to fully lithiated phase I and the results of lattice parameters and mass fraction of phases are summarized in Figure 9. Initial lattice parameters are for phase I: 8.1708 Å, phase II: 8.1248 Å, and phase III: 8.0170 Å. Under delithiation, the first phase transition proceeds when $0.76 < x_{Li} < 0.61$. This narrow interval reflects the rapid phase change and corresponds to the measurement of disordered sample $Li_{0.5}Ni_{0.5}Mn_{1.5}O_4$ prepared by molten-salt synthesize route with annealing at 720 °C [9]. Similarity with this study exhibits also the second phase transition between phase II/phase III which seems to be more gradual and was detected for $0.51 < x_{Li} < 0.21$. In our measurement, the beginning of the second phase transition began earlier than in [9] and much earlier than in [8]. Our reported second transition phase II/ phase III is the only phase transition reported in studies [23] [24]. Unfortunately, these studies do not show the changes reflections from (511) plane which would be more convincing about structure changes two or three-phase transition. When we were looking for possible reasons why some authors report two-phase and others three-phase transition, we found that the two-phase transition was reported preferably in studies of materials where the amount of $Mn^{3+}$ was above 20 %, while the clear three-phase transition was shown by studies with significantly lower amounts of $Mn^{3+}$ below 10 %. This is supported by results measured on disordered $Li_{0.5}Ni_{0.3}Mn_{1.7}O_4$ where a reduced amount of Ni promotes the $Mn^{3+}$ content to 19.3 % and materials exhibit a clear two-phase transition that was confirmed on all studied reflection planes. This transition was moreover detected in the late stage of delithiation [9].

$Mn^{3+}$ content and ordering of the structure influence significantly the speed and fluency of the structural changes. In the case of well-ordered LMNO, phase transitions phase I/phase II and phase II/phase III follow each other [36] overlaps, or moreover, all three phases exist simultaneously [9] at a certain charge level during delithiation. This is the result of slow $Li^+$ kinetics in well-ordered structures and the exact position of the phases and their possible overlap will be influenced also by the speed of lithiation. Therefore, in the study [8] where they used charging rate approx. 0.2 C, phase I disappeared only at $x_{Li} < 0.25$ in the case of well-ordered LNMO while in our study it happened already at $x_{Li} < 0.51$.

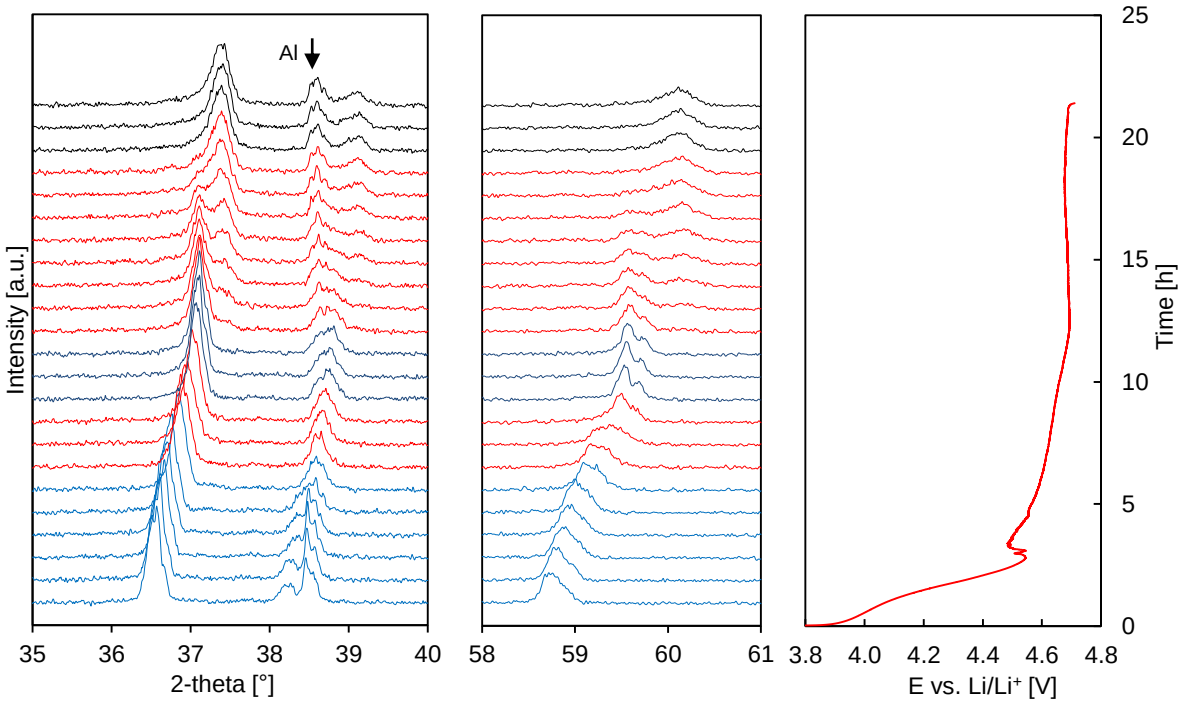


*Figure 7 XRD patterns (left) of LNMO obtained during delithiation process and corresponding voltage plateau (right) measured at C/20 load. Blue and black lines correspond to the occurrence of single-phase, red one indicates the presence of two phases simultaneously.*

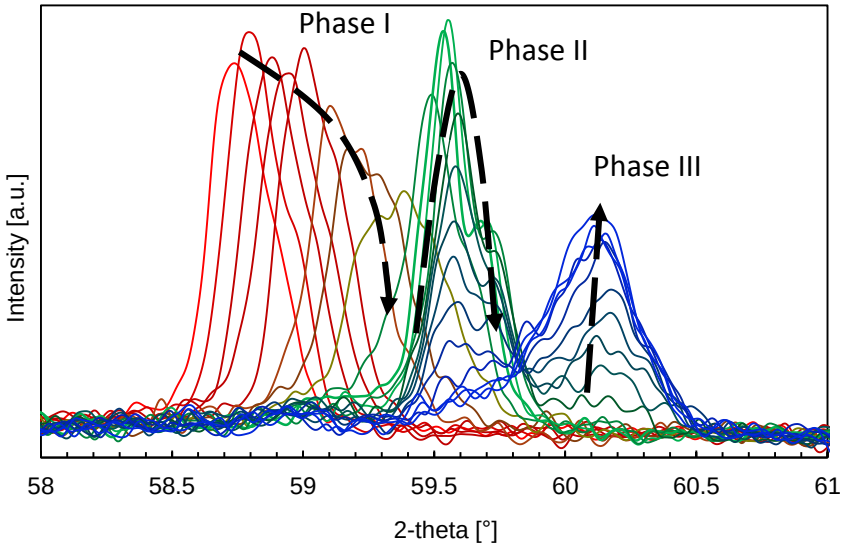


*Figure 8 Selected spectra of XRD patterns of LNMO reflection for (511) plane obtained during the delithiation process that clearly confirm the three-phase transition. Phase I: $LiNi_{0.5}Mn_{1.5}O_4$, phase II: $Li_{0.5}Ni_{0.5}Mn_{1.5}O_4$, and phase III: $Ni_{0.5}Mn_{1.5}O_4$.*

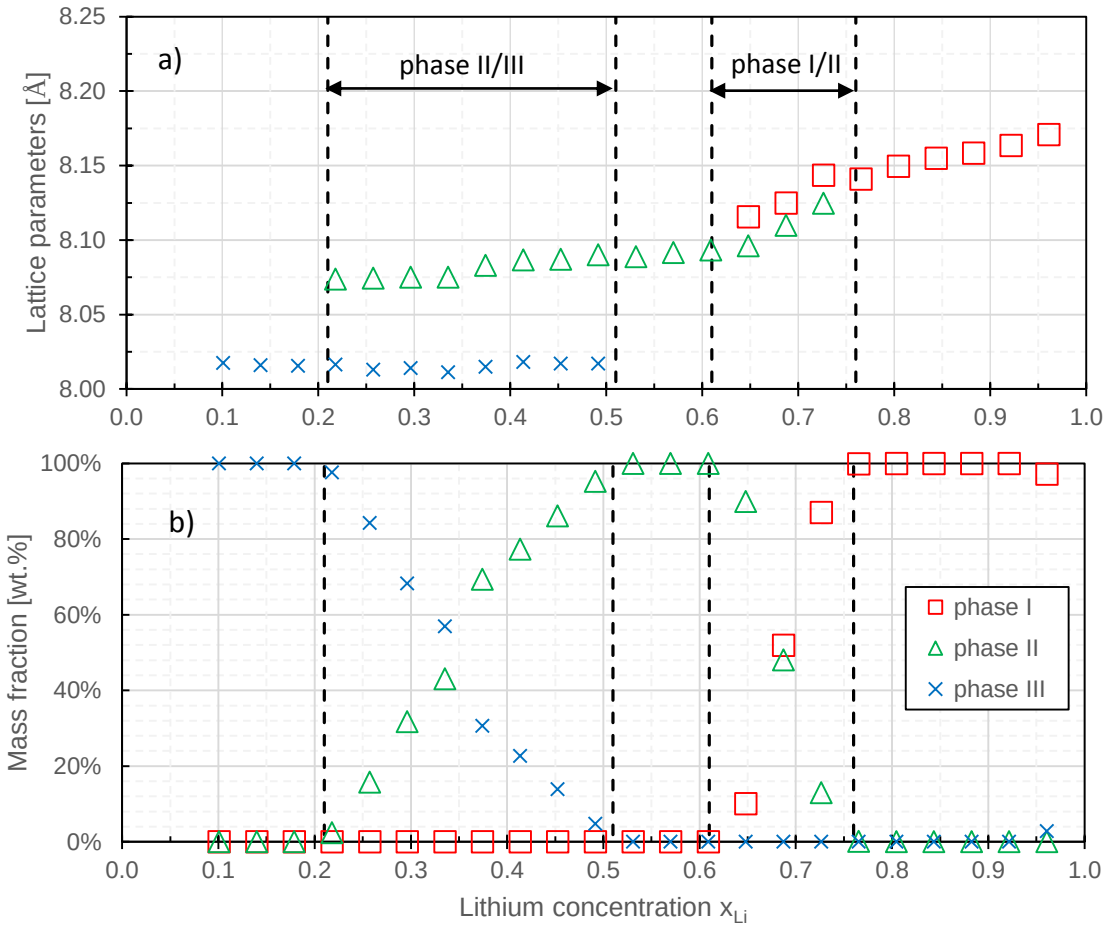


*Figure 9 Results from the Rietveld analysis of XRD spectra for LNMO for a different state of lithiation $x_{Li}$ obtained during delithiation at C/20 rate. a) Lattice parameter changes of identified phases I, II, and III b) Content ratio changes of the identified phases.*

**Phase transition in Cr-doped LNMO**

Diffraction spectra of Cr-doped LMNO in Figure 10 also exhibit the presence of a three-phase transition as was detected in the case of LNMO. All three phases exhibit again cubic Fd-3m symmetry. Phase I in a fully lithiated state corresponds to $LiCr_{0.1}Ni_{0.4}Mn_{1.5}O_4$, phase II can be attributed to partially delithiated $Li_{0.5}Cr_{0.1}Ni_{0.5}Mn_{1.5}O_4$ and Phase III is $Cr_{0.1}Ni_{0.5}Mn_{1.5}O_4$ corresponds to a fully charged state. The position of the phase transition area and corresponding lattice parameter changes are summarized in Figure 12. The first two-phase domain (for phase I/II) is present when $0.45 < x_{Li} < 0.72$ i.e. in the region where $Ni^{2+}$ is oxidized to $Ni^{3+}$ while phase II/III transition is much narrower and occurs when $0.2 < x_{Li} < 0.38$ which is accompanied mainly with $Ni^{3+}/Ni^{4+}$ oxidation process. It is evident that in both two-phases transitions the lattice parameters of transition phases are much closer than in undoped LNMO. This is partly because the Cr-doping increases the cell volume in a fully delithiated state (see Table 3) and thus reduced the volume changes of the lattice. On the other hand, this effect influenced only the phase II/III transition but the slightly closer lattice parameters were detected also during phase I/II transition. Increased lattice parameters in the lithiated state for Cr-doped LNMO could have a strongly positive effect on $Li^+$ diffusivity mainly at charged state because the larger interatomic distances at a similar element composition could importantly promote the diffusion of $Li^+$ in bulk. Significant influence of Cr-doping we detect also in case of position and length of individual phase transition. In the case of undoped LNMO, the two-

phase I/II region was sharp whereas the two-phase II/III region was gradual and fluent. Cr-doped LNMO showed opposite characteristics and thus whereas phase I/II transition is consuming broader delithiation range, transformation within phase II/III transition took place much faster. It could be said that accelerated transition kinetics were observed especially in the region closer to the intrinsic electrochemical activity of chromium i.e. in the region of $Ni^{3+}/Ni^{4+}$ redox couple where two-phase II/III transition occurred. A much slower phase transformation was observed in the initial phase of delithiation (phase I/II transition) and it can be a consequence of reduced structure ordering accompanied by lower $Mn^{3+}$ content. This is in good agreement with [9] where the same tendency exhibits the disordered $LiNi_{0.5}Mn_{1.5}O_4$ with the comparison with the ordered one. Especially faster phase II/III transition with reduced volume changes could help improve capacity retention at higher C-rates. Reduced volume changes resulting from larger lattice parameters in a fully delithiated state could moreover reduce the internal stress inside the particles at higher loads and it could, in turn, reduce the generation of microcracks and thus it makes the other beneficial influence to longer life-span of such battery systems.

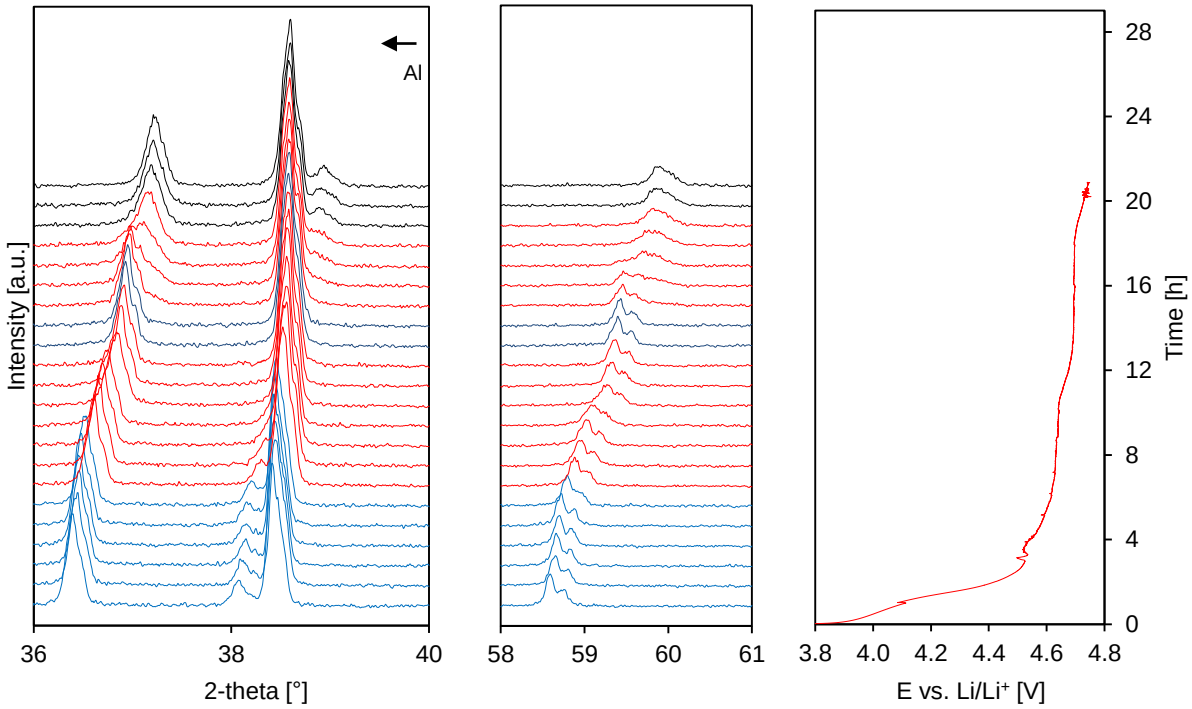


*Figure 10 XRD patterns (left) of Cr-doped LNMO obtained during delithiation process and corresponding voltage plateau (right) measured at C/20 load. Blue and black lines correspond to the occurrence of single-phase regions; red one indicates the presence of two phases simultaneously.*

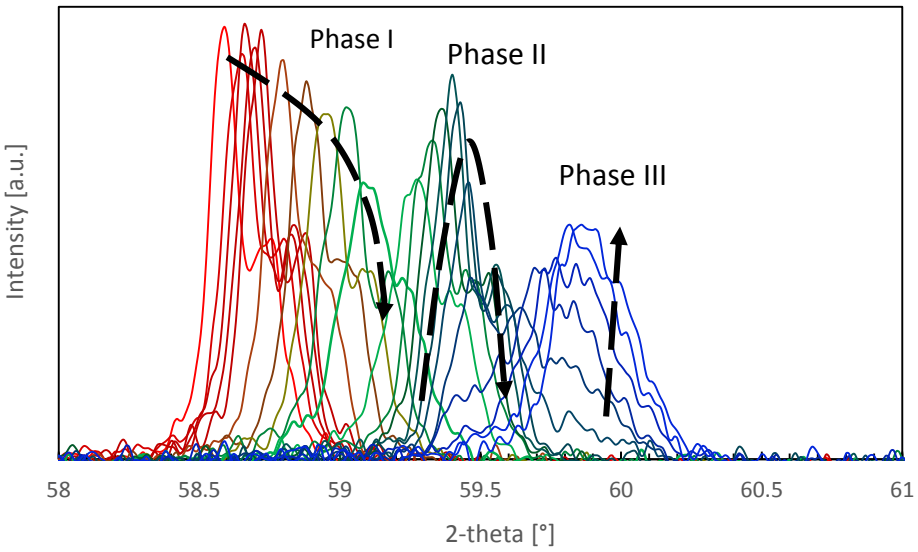


*Figure 11 Selected spectra of XRD patterns of Cr-doped LNMO obtained during the delithiation process that confirms the three-phase transition. Phase I: $LiCr_{0.1}Ni_{0.4}Mn_{1.5}O_4$, phase II: $Li_{0.5}Cr_{0.1}Ni_{0.4}Mn_{1.5}O_4$, and phase III: $Cr_{0.1}Ni_{0.5}Mn_{1.5}O_4$.*

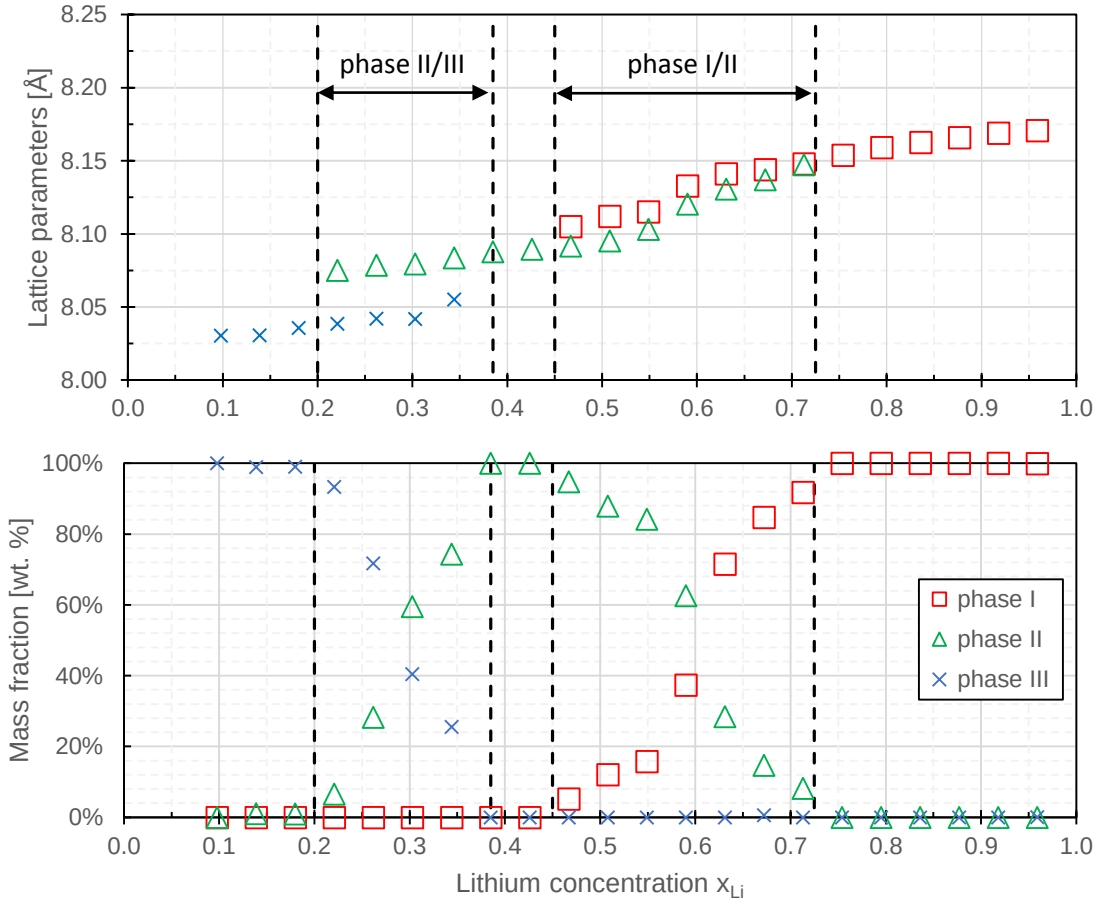


*Figure 12 Results from the Rietveld analysis of XRD spectra for LCNMO (Cr-doped LNMO) in a different state of lithiation $x_{Li}$: a) Lattice parameter changes of $LiCr_{0.1}Ni_{0.5}Mn_{1.5}O_4$ (phase I) corresponding to discharged state, $Li_{0.5}Cr_{0.1}Ni_{0.5}Mn_{1.5}O_4$ (phase II) and $Cr_{0.1}Ni_{0.5}Mn_{1.5}O_4$ (phase III) for partially and fully charged state b) Content ratio changes of the identified phases.*

*Table 3 Lattice parameters in lithiated and delithiated state of disordered LMO, LNMO, and LCNMO prepared by solid-state reaction.*

| Material | Lithiated | | Delithiated | |
|---|---|---|---|---|
| | Lattice par. [Å] | Lattice vol. [Å$^3$] | Lattice par. [Å] | Lattice vol. [Å$^3$] |
| $LiMn_2O_4$ | a= 8.2117 | 553.73 | a= 8.0493 | 521.52 |
| $LiNi_{0.5}Mn_{1.5}O_4$ | a= 8.1708 | 545.50 | a= 8.0176 | 515.39 |
| $LiCr_{0.1}Ni_{0.4}Mn_{1.5}O_4$ | a= 8.1705 | 545.44 | a= 8.0304 | 517.86 |

Figure 13 represents the summary of volume changes of characterized materials in comparison with similar materials LMO, LNMO, and Cu-doped LMNO prepared by the sol-gel technique [23] and also in comparison with our already published study focused on the well commercialized LFP cathode material [25]. In the case of LMO volume changes, the comparison indicates that these changes are more pronounced for materials prepared by the sol-gel synthesis method than those prepared by the solid-state synthesis. This has an origin in the lower lattice parameters of a fully lithiated structure for cathode material prepared by solid-phase synthesis. On the other hand, our LNMO exhibits lowering of volume changes which took place on the same scale as in the case of LMNO prepared by sol-gel synthesis [23]. A substitution of nickel by chromium brings further stabilization of the structure from the volume changes point of view and this improvement could therefore help to the long-term stability of the electrode system.

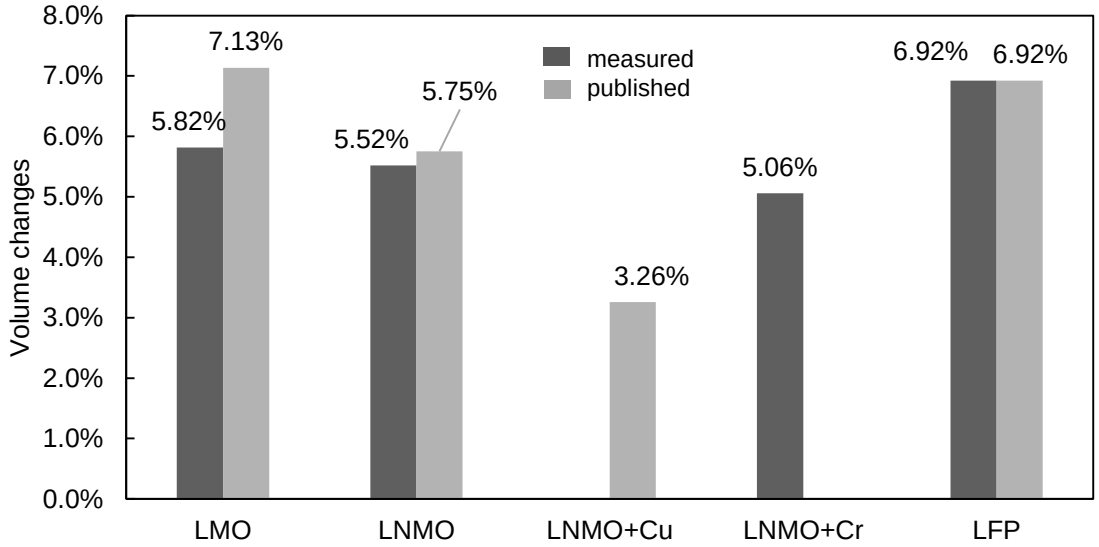


*Figure 13 Summary of volume changes of different disordered LMO-based cathode and commercial LFP [2], [25], [23]. Published LMO, LNMO, and Cu doped LNMO were prepared by sol-gel synthesis and our measured samples were prepared by solid-state reaction.*

**Lithium Diffusivity Study Using Electrochemical Impedance Spectroscopy**

To evaluate the effect of chromium doping on the diffusivity of lithium in the bulk of the active mass, electrochemical impedance spectroscopy (EIS) study of both materials was performed and the Nyquist diagrams, shown in Figure 14 were obtained. The EIS spectra show the impedance behavior of the electrodes in discharged (fully lithiated) state at potential $E$=2.86 V. The electrodes were subjected to two voltammetric cycles before EIS, therefore we assume that a significant part of the SEI layer was already formed. Spectra

comprised of a semicircle measured in the frequency range 100 kHz to 76 Hz, where the minimum of -*Z''* was measured, and of an inclined line at low-frequency range down to 100 mHz. The semicircle represents the charge transfer process and the inclined line represents the diffusion of lithium ions into the bulk of the electrode material. Diffusion is in the impedance response described by the Warburg coefficient $\sigma_w$ and in an equivalent circuit, this process represents the Warburg impedance component W2. Coefficient $\sigma_w$ can be obtained from the fit of the spectra by an equivalent circuit (typical equivalent circuit for fully discharge state is in Figure 15) or from the Eq. 2

$$Z' = R_{el} + R_{ct} + \sigma_w \omega^{-\frac{1}{2}} \quad (2)$$

where $R_{el}$ and $R_{ct}$ are the resistance of the electrolyte and the charge transfer resistance respectively and $\omega$ is the angular frequency in the low-frequency region. Coefficient $\sigma_w$ can be derived from the slope of the real part of impedance Z´ *vs*. the reciprocal square root of the angular frequencies ($\omega^{-1/2}$). The interpolated dependencies, including the equation of the linear interpolation, are shown in Figure 16. Per the findings of other authors who studied the diffusion properties of cathode materials such as $LiFePO_4$ [39], LiNiMnO [40], LiNiCoMnO [41] or Al, Mg, and Co-doped LiMnO [42], we use a similar approach to determine the diffusion coefficient $D_{Li+}$ that can be calculated from Eq. 3

$$D_{Li^+} = \frac{2R^2T^2}{c_{Li}^2 n^4 F^4 A^2 \sigma_w^2} \quad (3)$$

where $D_{Li+}$ represents the lithium diffusion coefficient, $R$ is the universal gas constant, $T$ is the absolute temperature in kelvin, $c_{Li}$ is the lithium concentration in the cathode material (calculated by as 23845 mol·m$^{-3}$), $n$ is the number of electrons transferred in charge transfer reaction, $F$ is the Faraday's constant, $A$ is electrode surface area and $\sigma_w$ is above mentioned the Warburg coefficient.

The exchange current density can be calculated then from Eq. 4:

$$j_0 = \frac{RT}{nFR_{ct}A} \quad (4)$$

Where $R_{ct}$ is the charge-transfer resistance and in this study were obtained by fitting the spectra using EC-lab analysis tools. An equivalent circuit in Figure 15 was used for the simulation of the spectra.

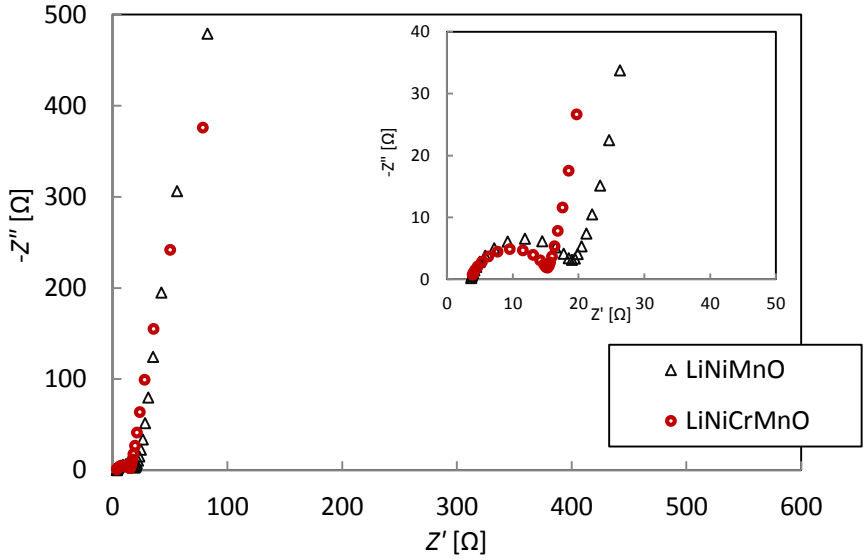

*Figure 14 EIS Nyquist plots of the electrode response in the frequency range 0.1 Hz – 100 kHz for LNMO and LCNMO*

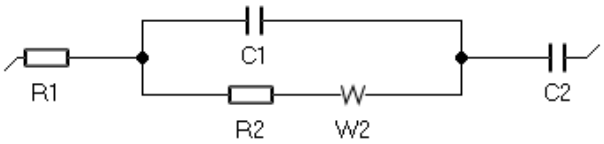


*Figure 15 Equivalent circuit for simulation of impedance behavior of the electrodes – response in Figure 14*

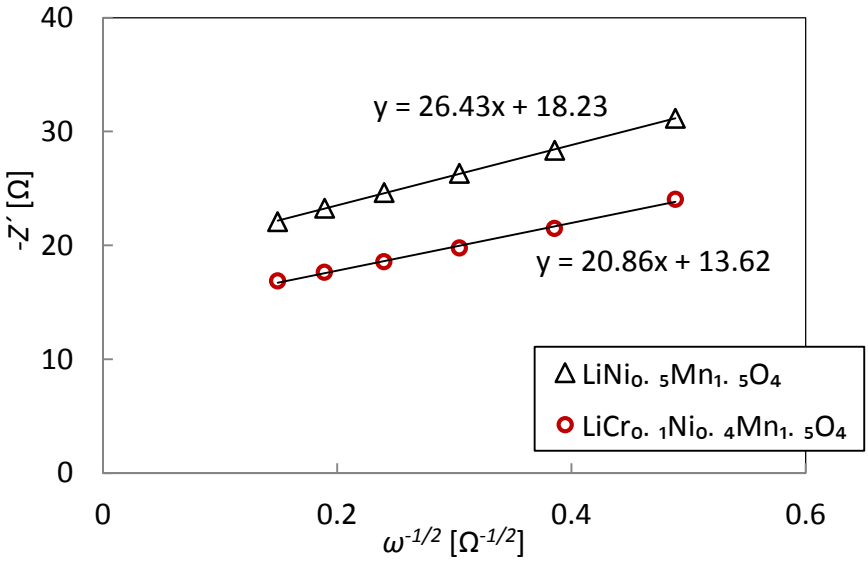


*Figure 16 The relationship between Z´ and $\omega^{-1/2}$ at low frequencies for LNMO and LCNMO*

Table 4 contains the values of $R_{ct}$, double-layer capacitance $C_{dl}$, Warburg coefficient $\sigma_{w,}$ and also the values of calculated diffusion coefficient $D_{Li+}$ and exchange current density $j_0$. Diffusion coefficients were calculated both from the values of the electrode area denoted as $D_{Li+\ el}$ and from the value of the active surface area of the active substance denoted as $D_{Li+\ as}$ according to Table 1. The diffusion coefficient in our calculation reaches value $1.45\times10^{-14}$ $cm^2s^{-1}$ for LNMO in a full discharge state which is in good agreement with the result for LMO in the study [42] and is a much higher value than in the case of Co-doped LNMO in the study [40] whose authors also use the electrode area. Typical results of the GITT technique bring the values in the range of order $10^{-10}$ – $10^{-12}$ $cm^2s^{-1}$ for all states of charge of LMNO [40]. It has to be noted that the results of different authors vary depending on what surface area was used for the calculation as well as on what description of concentration of lithium inside of the electrode was selected (concentration of Li in bulk or electrolyte soaked into electrode mass). Although there are different approaches in different studies, it has to be concluded that this method can be still used for the comparison of materials within the scope of each individual publication. From our calculation of the diffusion coefficient and the exchange current density, we can conclude that Cr-doping of LMNO increases diffusion values inside the bulk of material as well as the activity of such improved material expressed by the higher value of the exchange current density. This fully corresponds with the improved performance of the Cr-doped LNMO during a high rate of 5 C cycling [30].

*Table 4* Nyquist analysis of LNMO and Cr-doped LNMO cathode in a discharged state in the second cycle

| | $R_e$ [Ω] | $C_{dl}$ [F] | $R_{ct}$ [Ω] | $\sigma_w$ [Ω Hz$^{-1/2}$] | $C_L$ [F] | $D_{Li+\,el}$ [cm$^2$s$^{-1}$] | $D_{Li+\,as}$ [cm$^2$s$^{-1}$] | $j_0$ [A cm$^{-2}$] |
|---|---|---|---|---|---|---|---|---|
| **$LiNi_{0.5}Mn_{1.5}O_4$** | 4.795 | $1.29\cdot10^{-5}$ | 13.11 | 28.81 | $3.60\cdot10^{-3}$ | $1.45\cdot10^{-14}$ | $5.69\cdot10^{-17}$ | $7.89\cdot10^{-4}$ |
| **$LiCr_{0.1}Ni_{0.4}Mn_{1.5}O_4$** | 4.177 | $9.72\cdot10^{-6}$ | 10.05 | 18.95 | $4.44\cdot10^{-3}$ | $2.32\cdot10^{-14}$ | $7.47\cdot10^{-17}$ | $1.03\cdot10^{-3}$ |

The graph of discharge capacities in Figure 18 b) shows the performance of the electrodes in the first 65 cycles and under different C rates. Cr-doped LNMO exhibits a much higher discharging capacity especially at the highest 5 C rate despite larger particle diameters and smaller active surface area. This can be explained mainly by different diffusivity inside the bulk of the active mass. During the 5 C rate, the LMNO exhibits a gradual increase of discharge capacities that could be attributed to some formation effect of the high rate cycling. To assess the changes in electrode diffusion properties, diffusion coefficients $D_{Li+}$ were evaluated also in a different state of galvanostatic cycling – after 30, 55, and 65 cycles when the electrodes were in a full discharged state. The slope of real impedance on the reciprocal square root of the angular frequencies ($\omega^{-1/2}$) for both materials is displayed in Figure 17. Corresponding diffusion coefficients $D_{Li+}$ calculated on the geometric electrode area are plotted above the galvanostatic dependencies in Figure 17 b). A significant decrease of $D_{Li+}$ after 30 cycles from the initial one can be easily explained by the different states of electrodes. Initial diffusion coefficients were measured in full discharge state when $x = 1$ for $Li_xNi_{0.5}Mn_{1.5}O_4$ or $Li_xNi_{0.4}Cr_{0.1}Mn_{1.5}O_4$ whereas after 30 cycles of 0.5 C rate some residual charge remain in the material and therefore x<1. According to [23], a decrease of almost two orders of $D_{Li+}$ can be expected when the state of charge increases by about 20 % at the start of charging. LNMO exhibits a much higher drop of $D_{Li+}$ which could be due to a lower degree of active mass lithiation in the discharged state. Another evaluation of the diffusion coefficient was after high rate cycling - 55 cycles and after 65 cycles. A partial increase of the diffusion coefficient for both electrodes was detected already at the end of the high-rate test where the discharge rate was 1 C and mainly after the end of cycling, where the same state of lithiation is expected as before the high-rate cycling. It can be concluded that the diffusion coefficient was higher for Cr-doped LNMO in each state of galvanostatic cycling and also that high-rate cycling helps to increase the diffusion coefficient inside the electrode mass.

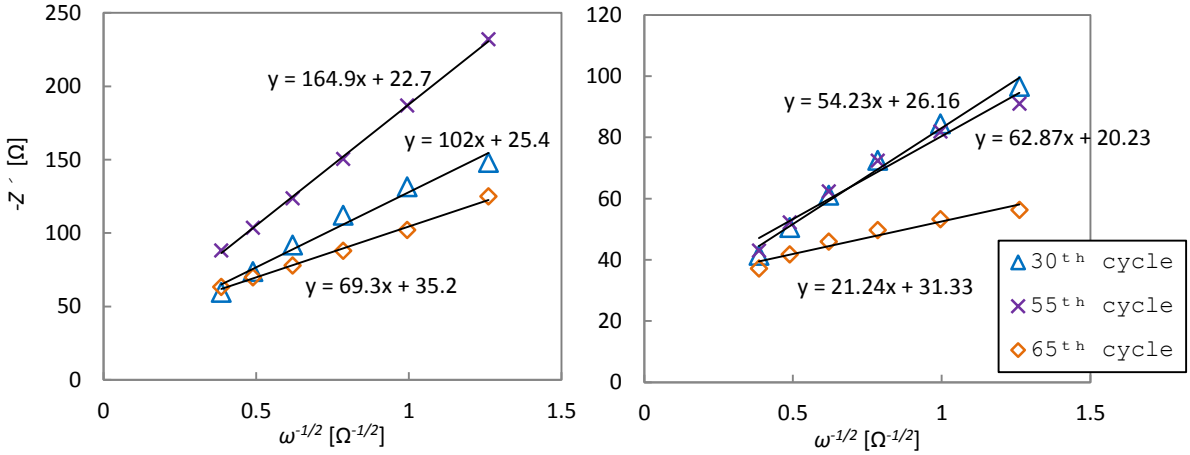


*Figure 17 The relationship between Z´ and $\omega^{-1/2}$ at low frequencies for LNMO (left) and Cr doped LNMO (right)*

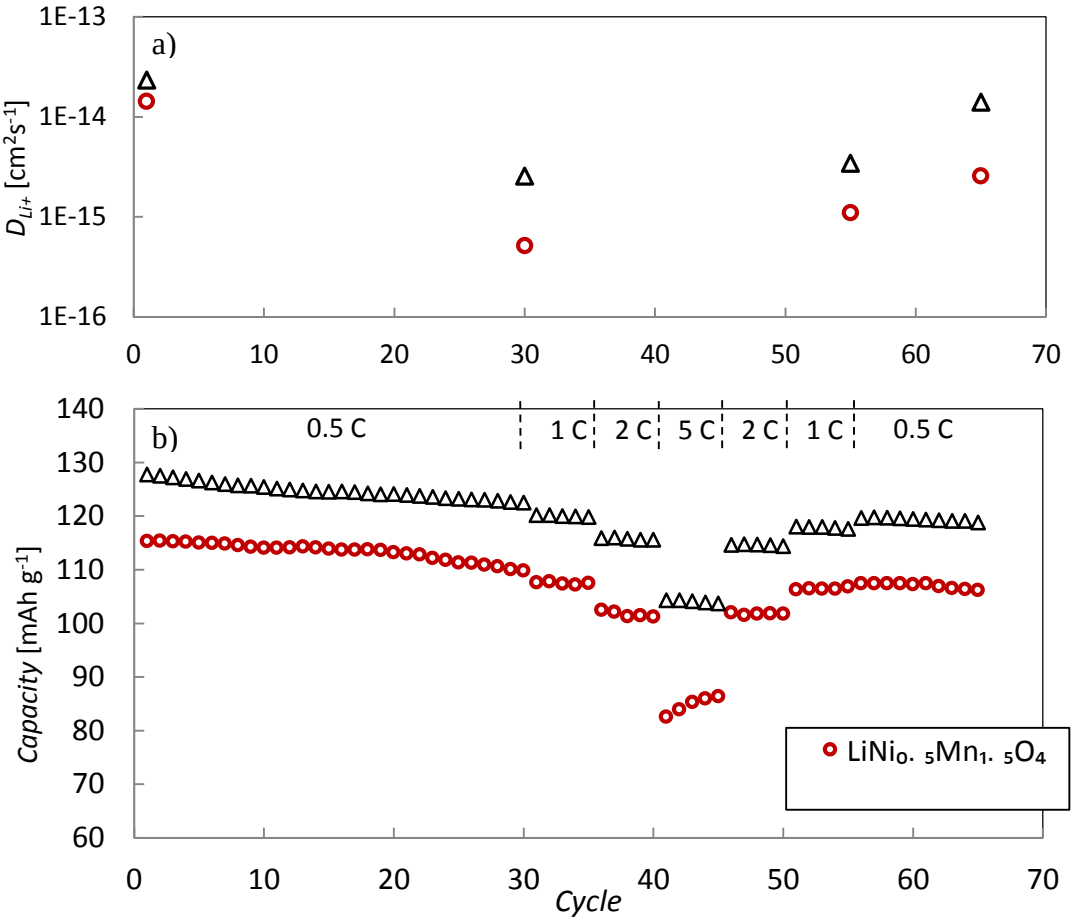


*Figure 18 Values of a) calculated diffusion coefficients for LNMO and LCNMO in the corresponding state of galvanostatic cycling b) discharge capacities during cycling with high-rate galvanostatic test*

## Conclusions

LMO ($LiMn_2O_4$), LNMO ($LiNi_{0.5}Mn_{1.5}O_4$), and LCNMO ($LiCr_{0.1}Ni_{0.4}Mn_{1.5}O_4$) prepared by solid-state synthesis were characterized by in-situ X-ray spectroscopy, and the effect of chromium doping was evaluated by electrochemical impedance spectroscopy. The *in-situ* XRD technique gives a detailed insight into the lattice parameter changes as well as the results elucidate the phase changes during the delithiation of the electrode. All synthesized structures exhibit disordered structure with Fd-3m space group symmetry.

Among the main detected changes for LMO, need to be mentioned the smaller lattice parameters in a fully lithiated state in the case of solid-state synthesis compared to sol-gel, resulting in lesser volume changes [23]. LNMO material prepared by solid-state synthesis at 700 °C exhibits approx. 14 % $Mn^{3+}$ content and the potential difference of nickel redox pairs reached 58 mV confirming the strongly disordered nature of the material. Although LNMO contains such high $Mn^{3+}$ content and highly disordered structure, the in-situ X-ray Rietveld analysis has been able to recognize three-phase transition during delithiation. Comparison of the cathode behavior and phase evolution of our disordered LNMO material prepared by solid-state synthesis with materials prepared by the sol-gel technique with higher $Mn^{3+}$ content revealed differences mainly in presence of second transition phases $Li_{0.5}Ni_{0.5}Mn_{1.5}O_4$.

Chromium doping of LNMO influences both $Mn^{3+}$ content and the disordering of the structure. Whereas the $Mn^{3+}$ content was reduced by 37 %, nickel redox plateaus

showed greater potential separation and thus point to a further increase in the disordering of the structure. LCNMO also stabilized the structure changes in several aspects. First of all, it increased the lattice parameters of the fully delithiated phase and thus effectively reduced the volume changes during cycling. Second, the position and width of both two-phase regions change in comparison with LNMO. For undoped LNMO, the two-phase I/II region was narrow and sharp whereas the two-phase II/III region was gradual and much broader. Cr-doped LNMO showed a completely opposite characteristic and thus whereas phase I/II transition is consuming broader delithiation range, transformation within phase II/III transition took place much faster. However, chromium doping, unlike other doping elements, is not able to reduce this three-phase change to two- or one-phase.

The impedance study supplemented by evaluation of the diffusion coefficient revealed the improved diffusivity of Li in Cr-doped LNMO in the discharged (fully lithiated) state, and during cycling, the chromium further intensifies the positive effect on diffusion properties, which results in much higher discharge capacities mainly at high-rate cycling. Effect of some kind of "formation" of an electrode from a diffusivity point of view under high rate cycling was observed for the LNMO cathode material.

Doping of $LiNi_{0.5}Mn_{1.5}O_4$ thus represents a very promising way in terms of improving structural stability, diffusivity, and also durability of high-voltage batteries. Further research on other materials or different approaches while synthesizing materials are needed to improve the performance of batteries based on LNMO.

## Acknowledgment

This research work has been carried out in the Centre for Research and Utilization of Renewable Energy (CVVOZE). This work was supported by the specific graduate research of the Brno University of Technology No. FEKT-S-20-6206.

## References

[1] J. Harlow, X. Ma, J. Li, E. Logan, Y. Liu, N. Zhang, L. Ma, S. Glazier, M. Cormier, M. Genovese, S. Buteau, A. Cameron, J. Stark and J. Dahn, "A Wide Range of Testing Results on an Excellent Lithium-Ion Cell Chemistry to be used as Benchmarks for New Battery Technologies", *Journal of The Electrochemical Society*, vol. 166, no. 13, pp. A3031-A3044, 2019.

[2] A. Padhi, K. Nanjundaswamy and J. Goodenough, "Phospho-olivines as Positive-Electrode Materials for Rechargeable Lithium Batteries", *Journal of The Electrochemical Society*, vol. 144, no. 4, pp. 1188-1194, 1997.

[3] A. Yamada, S. Chung and K. Hinokuma, "Optimized LiFePO4 for Lithium Battery Cathodes", *Journal of The Electrochemical Society*, vol. 148, no. 3, pp. A224-A229, 2001.

[4] Y. Gao, K. Myrtle, M. Zhang, J. Reimers and J. Dahn, "Valence band of LiNi x Mn 2 − x O 4 and its effects on the voltage profiles of LiNi x Mn 2 − x O 4 /Li electrochemical cells", *Physical Review B*, vol. 54, no. 23, pp. 16670-16675, 1996.

[5] J. Xu, S. Dou, H. Liu and L. Dai, "Cathode materials for next generation lithium ion batteries", *Nano Energy*, vol. 2, no. 4, pp. 439-442, 2013.

[6] H. Yoo, E. Markevich, G. Salitra, D. Sharon and D. Aurbach, "On the challenge of developing advanced technologies for electrochemical energy storage and conversion", *Materials Today*, vol. 17, no. 3, pp. 110-121, 2014.

[7] J. Kim, S. Myung, C. Yoon, S. Kang and Y. Sun, "Comparative Study of LiNi 0.5 Mn 1.5 O 4 - δ and LiNi 0.5 Mn 1.5 O 4 Cathodes Having Two Crystallographic Structures", *Chemistry of Materials*, vol. 16, no. 5, pp. 906-914, 2004.

[8] J. Zheng, J. Xiao, X. Yu, L. Kovarik, M. Gu, F. Omenya, X. Chen, X. Yang, J. Liu, G. Graff, M. Whittingham and J. Zhang, "Enhanced Li ion transport in LiNi0.5Mn1.5O4 through control of site disorder", *Physical Chemistry Chemical Physics*, vol. 14, no. 39, 2012.

[9] H. Duncan, B. Hai, M. Leskes, C. Grey and G. Chen, "Relationships between Mn 3 Content, Structural Ordering, Phase Transformation, and Kinetic Properties in LiNi x Mn 2– x O 4 Cathode Materials", *Chemistry of Materials*, vol. 26, no. 18, pp. 5374-5382, 2014.

[10] T. Kazda, J. Vondrák, A. Visintin, M. Sedlaříková, J. Tichý and P. Čudek, "Electrochemical performance of Mo doped high voltage spinel cathode material for lithium-ion battery", *Journal of Energy Storage*, vol. 15, pp. 329-335, 2018.

[11] H. Jahn and E. Teller, "Stability of polyatomic molecules in degenerate electronic states - I—Orbital degeneracy", *Proceedings of the Royal Society of London. Series A - Mathematical and Physical Sciences*, vol. 161, no. 905, pp. 220-235, 1937.

[12] Y. Xie, Y. Jin and L. Xiang, "Understanding Mn-Based Intercalation Cathodes from Thermodynamics and Kinetics", *Crystals*, vol. 7, no. 7, 2017.

[13] Y. Hou, K. Chang, H. Tang, B. Li, Y. Hou and Z. Chang, "Drastic enhancement in the rate and cyclic behavior of LiMn2O4 electrodes at elevated temperatures by phosphorus doping", *Electrochimica Acta*, vol. 319, pp. 587-595, 2019.

[14] P. Chand, V. Bansal, . Sukriti and V. Singh, "Investigations of spinel LiZnxMn2−xO4 ($x \leq 0.03$) cathode materials for a lithium ion battery application", *Materials Science and Engineering: B*, vol. 238-239, pp. 93-99, 2018.

[15] Z. Su, Z. Lu, X. Gao, P. Shen, X. Liu and J. Wang, "Preparation and electrochemical properties of indium- and sulfur-doped LiMnO2 with orthorhombic structure as cathode materials", *Journal of Power Sources*, vol. 189, no. 1, pp. 411-415, 2009.

[16] W. Pang, J. Lee, Y. Wei and S. Wu, "Preparation and characterization of Cr-doped LiMnO2 cathode materials by Pechini's method for lithium ion batteries", *Materials Chemistry and Physics*, vol. 139, no. 1, pp. 241-246, 2013.

[17] K. Vediappan, K. Prasanna, S. Shanmugan, R. Gnanamuthu and C. Lee, "Structural stability and electrochemical properties of gadolinium-substituted LiGd x Mn 2-x O 4 spinel as cathode materials for Li-ion rechargeable batteries", *Applied Surface Science*, vol. 449, pp. 412-420, 2018.

[18] S. Bhuvaneswari, U. Varadaraju, R. Gopalan and R. Prakash, "Structural stability and superior electrochemical performance of Sc-doped LiMn2O4 spinel as cathode for lithium ion batteries", *Electrochimica Acta*, vol. 301, pp. 342-351, 2019.

[19] L. Chen, H. Wu, H. Wang, L. Chen, X. Pu and Z. Chen, "Tailoring NaVO3 as a novel stable cathode for lithium rechargeable batteries", *Electrochimica Acta*, vol. 307, pp. 224-231, 2019.

[20] X. Jian, J. Tu, Y. Qiao, Y. Lu, X. Wang and C. Gu, "Synthesis and electrochemical performance of LiVO3 cathode materials for lithium ion batteries", *Journal of Power Sources*, vol. 236, pp. 33-38, 2013.

[21] A. Slesarenko, I. Yakuschenko, V. Ramezankhani, V. Sivasankaran, O. Romanyuk, A. Mumyatov, I. Zhidkov, S. Tsarev, E. Kurmaev, A. Shestakov, O. Yarmolenko, K.

Stevenson and P. Troshin, "New tetraazapentacene-based redox-active material as a promising high-capacity organic cathode for lithium and potassium batteries", *Journal of Power Sources*, vol. 435, 2019.

[22] G. Sun, Y. Hu, Y. Sha, C. Shi, G. Yin, H. Zhang, H. Liu and Q. Liu, "An insoluble naphthalenediimide derivative as a highly stable cathode material for lithium-ion batteries", *Materials Chemistry and Physics*, vol. 236, 2019.

[23] Ł. Kondracki, A. Kulka, A. Milewska and J. Molenda, "In-situ structural studies of manganese spinel-based cathode materials", *Electrochimica Acta*, vol. 227, pp. 294-302, 2017.

[24] C. Gao, H. Liu, S. Bi, H. Li and C. Ma, "Investigation the improvement of high voltage spinel LiNi0.5Mn1.5O4 cathode material by anneal process for lithium ion batteries", *Green Energy & Environment*, 2020.

[25] L. Chladil, D. Kunický, P. Vanýsek and O. Čech, "In-Situ X-Ray Study of Carbon Coated LiFePO 4 for Li-Ion Battery in Different State of Charge", *ECS Transactions*, vol. 87, no. 1, pp. 107-114, 2018.

[26] J. Yoon, D. Kim, J. Um, M. Jeong, W. Oh and W. Yoon, "Effect of local structural changes on rate capability of LiNi 0.5 Mn 1.5 O 4−δ cathode material for lithium ion batteries", *Journal of Alloys and Compounds*, vol. 686, pp. 593-600, 2016.

[27] Y. Shen, X. Ju, J. Zhang, T. Xie, F. Zong, D. Xue, X. Lin, J. Zhang and Q. Li, "A convenient co-precipitation method to prepare high performance LiNi0.5Mn1.5O4 cathode for lithium ion batteries", *Materials Chemistry and Physics*, vol. 240, 2020.

[28] X. Ren, Y. Wang, Q. Xiao, G. Lei and Z. Li, "Excellent electrochemical performances of high-voltage LiNi0.5Mn1.5O4 hollow microspheres synthesized by a static co-precipitation method", *Materials Letters*, vol. 248, pp. 97-100, 2019.

[29] T. Kazda, J. Tichý, O. Cech, M. Sedlarikova, P. Čudek, T. Binar, J. Švarc and P. Vyroubal, "Influence of Conditions on the Process of Spinel Based Cathode Material Synthesis", *ECS Transactions*, vol. 81, no. 1, pp. 127-133, 2017.

[30] T. Kazda, O. Cech, J. Vondrak, A. Strakova Fedorkova, A. Visintin, P. Cudek and V. Kasparek, "Comparative Study of the Properties of High Voltage Spinel Cathode Material Depending on the Method of Synthesis", *ECS Transactions*, vol. 63, no. 1, pp. 15-21, 2014.

[31] E. Logan, E. Tonita, K. Gering, L. Ma, M. Bauer, J. Li, L. Beaulieu and J. Dahn, "A Study of the Transport Properties of Ethylene Carbonate-Free Li Electrolytes", *Journal of The Electrochemical Society*, vol. 165, no. 3, pp. A705-A716, 2018.

[32] M. Börner, P. Niehoff, B. Vortmann, S. Nowak, M. Winter and F. Schappacher, "Comparison of Different Synthesis Methods for LiNi 0.5 Mn 1.5 O 4 -Influence on Battery Cycling Performance, Degradation, and Aging", *Energy Technology*, vol. 4, no. 12, pp. 1631-1640, 2016.

[33] W. Zhu, D. Liu, J. Trottier, P. Hovington, C. Gagnon, A. Guerfi, K. Zaghib, A. Mauger, H. Groult and C. Julien, "In Situ XRD Study of the Phase Evolution in LixMn1.5Ni0.5O4 as 4.7-Volt Positive Electrode Materials for Li-Ion Batteries", *ECS Transactions*, vol. 58, no. 14, pp. 35-40, 2014.

[34] S. GURPREET, P. AMRISH, S. ANJAN and G. SUDIPTO, "Synthesis and characterization of citric acid assisted Cr doped lithium manganese oxide spinel", *Ceramics – Silikáty*, vol. 53, no. 4, pp. 260-267, 2009.

[35] D. Liu, J. Hamel-Paquet, J. Trottier, F. Barray, V. Gariépy, P. Hovington, A. Guerfi, A. Mauger, C. Julien, J. Goodenough and K. Zaghib, "Synthesis of pure phase disordered LiMn1.45Cr0.1Ni0.45O4 by a post-annealing method", *Journal of Power Sources*, vol. 217, pp. 400-406, 2012.

[36] W. Zhu, D. Liu, J. Trottier, C. Gagnon, A. Mauger, C. Julien and K. Zaghib, "In-situ X-ray diffraction study of the phase evolution in undoped and Cr-doped LixMn1.5Ni0.5O4 ($0.1 \leq x \leq 1.0$) 5-V cathode materials", *Journal of Power Sources*, vol. 242, pp. 236-243, 2013.

[37] J. Hunter, "Preparation of a new crystal form of manganese dioxide: λ-MnO2", *Journal of Solid State Chemistry*, vol. 39, no. 2, pp. 142-147, 1981.

[38] C. Gao, H. Liu, S. Bi, H. Li and C. Ma, "Investigation the improvement of high voltage spinel LiNi0.5Mn1.5O4 cathode material by anneal process for lithium ion batteries", vol. 6, no. 1, pp. 114-123, 2021.

[39] Y. Cui, X. Zhao and R. Guo, "Improved electrochemical performance of La0.7Sr0.3MnO3 and carbon co-coated LiFePO4 synthesized by freeze-drying process", *Electrochimica Acta*, vol. 55, no. 3, pp. 922-926, 2010.

[40] M. Mohamedi, "Electrochemical investigation of LiNi0.5Mn1.5O4 thin film intercalation electrodes", *Electrochimica Acta*, vol. 48, no. 1, pp. 79-84, 2002.

[41] L. Wang, J. Zhao, X. He, J. Gao, J. Li, C. Wan and C. Jiang, "Electrochemical Impedance Spectroscopy (EIS) Study of LiNi1/3Co1/3Mn1/3O2 for Li-ion Batteries", *International Journal of Electrochemcal Science*, vol. 7, no. 1, pp. 345 - 353, 2012.

[42] C. Snyders and E. Ferg, "Electrochemical Impedance Spectroscopy (EIS) study of doped spinel manganese cathode oxide materials synthesized for Li-ion batteries", *Materials Today: Proceedings*, vol. 5, no. 4, pp. 10450-10459, 2018.

592
593